

Article

Study on Experimental and Constitutive Model of Granite Gneiss under Hydro-Mechanical Properties

Lin Liu ^{1,2} and Bo Wen ^{3,*} 

¹ Key Laboratory of Coastal Disaster and Defence, Ministry of Education, Hohai University, Nanjing 210024, China; linliunj@hotmail.com

² College of Harbour, Coastal and Offshore Engineering, Hohai University, Nanjing 210024, China

³ School of Engineering Audit, Nanjing Audit University, Nanjing 211815, China

* Correspondence: bowennj@hotmail.com

Abstract: Permeability, as a critical element in making sure the underground facilities are secure, is a vital consideration in analyzing the rock material seepage. Selecting granite gneiss from underground oil storage as the research sample in this study. Triaxial mechanical property tests under different hydro-mechanical properties were carried out under the rock full-automatic triaxial servo system that controls the application of axial pressure, confining pressure, and seepage pressure. Through experiments carried out, we obtained the rock samples' mechanical properties and permeability in three stages of the stress–strain process. The study shows that the seepage pressure considerably affects granite gneiss strength and deformation parameters under hydro-mechanical properties. On the basis of the same confining pressure, in pace with the growth in seepage pressure, elastic modulus, the deformation modulus, and the peak strength present a prominent decreasing inclination. The derived mechanical parameters are bound up with the stages we divided. This study analyzes and discusses the relationship among the strains and permeability, establishing the granite gneiss hydro-mechanical coupling constitutive model. Verification shows the results in numerical and experimental matches well, indicating that the rock hydro-mechanical properties could be effectively represented by the constitutive model.

Keywords: granite gneiss; hydro-mechanical properties; permeability; constitutive model



Citation: Liu, L.; Wen, B. Study on Experimental and Constitutive Model of Granite Gneiss under Hydro-Mechanical Properties. *Appl. Sci.* **2023**, *13*, 12130. <https://doi.org/10.3390/app132212130>

Academic Editor: Tiago Miranda

Received: 6 October 2023

Revised: 30 October 2023

Accepted: 6 November 2023

Published: 8 November 2023



Copyright: © 2023 by the authors. Licensee MDPI, Basel, Switzerland. This article is an open access article distributed under the terms and conditions of the Creative Commons Attribution (CC BY) license (<https://creativecommons.org/licenses/by/4.0/>).

1. Introduction

Rock coupling characteristics of hydro-mechanical properties caused by seepage water have become a focus of current research in rock mechanics and engineering [1]. The rock (body) influences and interacts with the environment in terms of the coexisting crustal stress field, seepage field, chemistry, temperature, and other fields; it is in a dynamic balance, especially in interactions of all fields [2–4]. The hydro-mechanical properties in rock mean that variations in the stress field can cause differences in the inner microcracks and pores of the rock, as well as variations in pore pressure and permeability internal the rock; in the meanwhile, due to changes in pore pressure, the affection on permeate on the microcracks and pores of the rock inner structure changes, thereby reversing the rock internal stress field. The interactions and influences in the light of the rock hydro-mechanical properties play a prominent role in rock engineering safety and stability [5,6].

Granite gneiss is a metamorphic rock with comparatively high mechanical strength, compact construction, and low porosity [7]. Further understanding the granite gneiss mechanical behavior is of vital importance to guarantee the rock storage projects have secure and efficacious design and construction. Currently, experimental research about rock permeability characteristics mainly centers on a number of high-permeability rocks (for instance, sandstone or coal rock) [8–10]. There are a handful of studies on rock permeability characteristics with high strength and low porosity (such as granite or marble). In recent

years, domestic and foreign scholars have also achieved a substantial amount of research results on indoor uniaxial or triaxial hydro-mechanical properties tests of rocks using water as the permeable medium [11–17]. From this research, the rock permeability is mainly with regard to elements, for instance, the strain, stress, fluid, pore pressure, and temperature, with the main research object being rocks with larger pores. The permeability of low-permeability hard rocks is rarely involved. Moreover, previous research mainly centered on the association between permeability and axial strain, with small amounts of research studies detailing the quantitative relationship among circumferential, volumetric strain, and rock permeability [18,19].

The rock's mechanical behavior can be represented by the constitutive model on rocks [20]. The constitutive model is an effective way to research the rock coupling characteristics in a water environment. The central research methods include applying empirical equations to test results directly, parallel connections of assorted components, as well as adding nonlinear terms. In view of the elastic–plastic theoretical framework, there were three sorts of rock constitutive models [21–23]. By simulating the influence of seepage in rocks on their deformation behavior under stress, the permeate influence on the rock's inner stress field can effectively be achieved. By characterizing the internal permeability evolution law of rocks through the deformation behavior under stress, the stress field effect on the seepage field can be achieved, thereby achieving the hydro-mechanical properties of rock. This research is beneficial for considering the study of rock mechanical properties, failure mechanisms, and evolution laws of seepage characteristics under the coupling state of a seepage environment and stress. It also provides a considerable reference for the security and perdurable stability of major national infrastructure items, that is, water conservancy and hydropower engineering, underground energy storage, as well as transportation engineering.

2. Materials and Methods

2.1. Basic Physical Characteristics of Granite Gneiss

Granite gneiss rock sample is taken from an underground oil storage cavern, which is from late Proterozoic. Its cardinal mineral components are plagioclase, hornblende, biotite, potassium feldspar, quartz, and so on, with high strength, brittleness, and hardness, making it a hard rock. In line with the recommendations of the International Society for Rock Mechanics (ISRM) [24], choosing standard cylindrical specimens that are 100 mm in height and 50 mm in diameter.

Rock sample density measurement involves soaking a dry rock sample in water, measuring the volume of water discharged, and then dividing the mass by the volume to obtain the rock density. The determination of rock porosity involves soaking dry rock samples in water and using a vacuum pump to saturate the rock samples. By measuring the weight difference between the saturated rock samples and dry rock samples, calculating the rock samples porosity. It was found that the average porosity of the rock sample is 1.79%, and the average natural density is 2.61 g cm^{-3} . It belongs to a low-permeability rock type, with a lower porosity and higher initial density.

2.2. Experiment Plan and Method

The fully automatic triaxial servo system for rocks could control axial pressure, confining pressure, and seepage pressure, as shown in Figure 1. Different seepage pressures are set at the rock sample at both ends so as to form seepage pressure differences to achieve the application of seepage pressure. The control system of seepage water pressure can accurately dominate the inlet seepage pressure, achieve the constant-flow pump method, and convert the rock sample permeability by monitoring the seepage water flow rate. The range of applied load for hydraulic pumps controlling the confining pressure is 0–60 MPa, and applied bias pressure range for hydraulic pumps controlling the axial pressure is 0–500 MPa. A linear displacement sensor (LVDT) and a circumferential strain measurement ring composed the strain measurement system. The experimental data can

be recorded in real-time and transmitted to the computer to achieve full digitalization and mapping during the experimental process, facilitating real-time dynamic monitoring of the experiment.



Figure 1. The fully automatic triaxial servo system for rocks.

Before starting the experiment, a rock saturation test was conducted to simulate the rock sample's natural state, as the granite gneiss had been in a saturated state when it was taken from an underground, underwater cavern. In order to decline the temperature changes during the experiment, maintain the indoor temperature at 20 ± 0.5 °C; this temperature is the basic requirement for room temperature testing [24]. The experiment adopted a loading method of stress control followed by strain control. At the initial loading stage, maintain the confining pressure and pore pressure values. Using 0.75 MPa/min loading rate, paying attention to observing the changes in the circumferential strain curve. When nonlinear characteristics are exhibited on the circumferential strain curve, the rock sample undergoes plastic deformation; that is, near the yield stress point, the loading method changed from stress control to strain control and controlled 0.01 mm/min loading rate till the rock sample failed. The two types of rock samples used for seepage pressure were 1 MPa and 3 MPa. The test plan is shown in Table 1.

Table 1. Axial creep strain in various coupled conditions.

		σ_3 (MPa)	
		4	6
Pore pressure/MPa	1	R1	R3
	3	R2	R4

Measuring the granite gneiss permeability in test accurately by the rock seepage water flow changes and its relationship with the confining pressure and pore pressure difference [25]. As shown in Formula (1):

$$K = \frac{\mu LV}{A \Delta P \Delta t}, \quad (1)$$

where K is the permeability (m^2); ΔP is the pore pressure difference between the specimen two ends (Pa); μ is the water dynamic viscosity ($\text{Pa}\cdot\text{s}$), $\mu = 1 \times 10^{-3}$ Pa·s at 20 °C; A is the rock specimen cross-sectional area (m^2); L is the rock specimen length (m); V is the instantaneous flow volume (m^3); and Δt is the time interval (s).

3. Results and Discussion

3.1. Stress–Strain Curve under Hydro-Mechanical Properties

The triaxial experimental research on the coupling effect of hydro-mechanical properties mainly centered on the stage before peak strength in the curve. The mechanical and deformation characteristics after the peak are relatively complex, and the seepage

transformed from the assumed continuous medium pore seepage to fracture seepage, and the seepage characteristics are also more complex. In order to describe the relevance and characteristics among the samples' axial, circumferential, and volumetric strains more clearly, the post-peak deformation stage was omitted, and only 1–2 experimental data points were left to indicate the peak points. The test's main mechanical and deformation parameters are presented in Table 2: σ_3 is confining pressure, P_i is the pore pressure, σ_c is peak strength, ϵ_{1c} is axial peak strain, ϵ_{3c} is circumferential peak strain, and E_s is the elastic modulus.

Table 2. The main mechanical and deformation parameters of the test.

Rock Sample	σ_3 /MPa	P_i /MPa	σ_c /MPa	$\epsilon_{1c}/10^{-3}$	$\epsilon_{3c}/10^{-3}$	E_s /GPa
R1	4	1	237.13	6.13	−4.51	44.91
R2		3	213.22	5.77	−3.60	39.24
R3	6	1	248.76	6.49	−4.73	51.02
R4		3	236.67	6.61	−4.31	40.27

The triaxial test stress–strain curve in the coupling effect is shown in Figure 2.

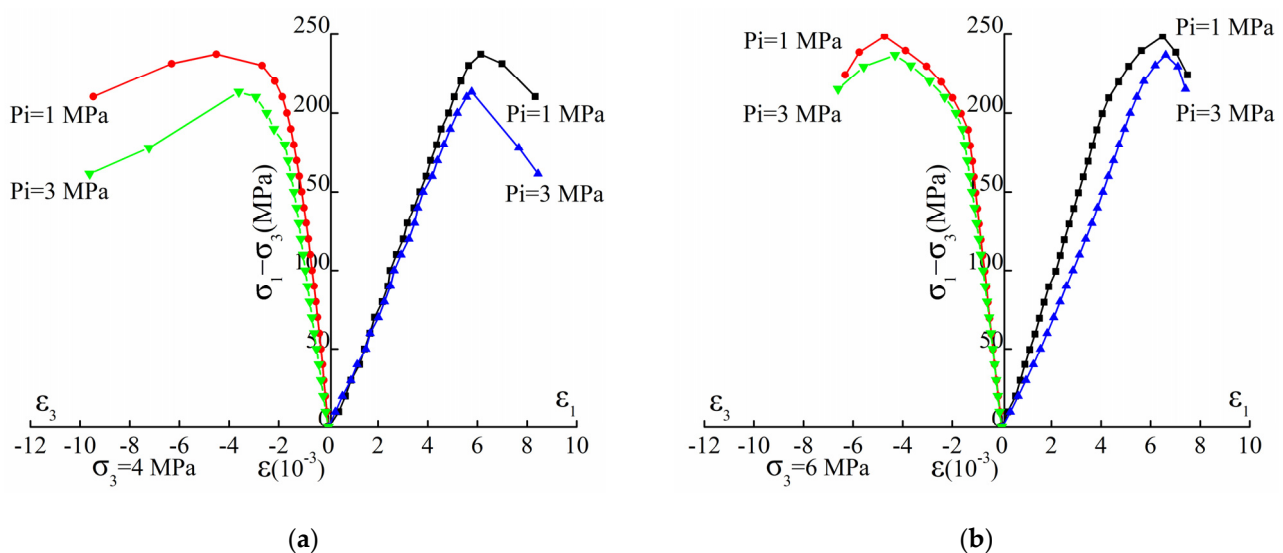


Figure 2. Triaxial compression tests stress–strain curves under hydro-mechanical properties: (a) $\sigma_3 = 4$ MPa; (b) $\sigma_3 = 6$ MPa.

From Figure 2, we can see that the rock samples generally go through three stages before failure. These stages are the microcrack compaction stage, the linear elastic deformation stage, and the internal damage expansion and deformation failure stage. The microcrack compaction stage is an early small nonlinear deformation stage in the stress application, which is caused by the closure of microcracks and pores inside rock samples in stress. After compacting the cracks, pores, and so on in the rock, the specimen enters the elastic deformation stage, which is a linear deformation stage mainly subject to the rock skeleton pressure, as well as its linear slope, which is the rock elastic modulus. This is in accordance with the results acquired in similar studies [26]. Subsequently, the specimen entered a relatively stable nonlinear deformation stage, followed by rapid deformation, reaching its peak strength. During this stage, the crack, along with the stress, increases stably. As the stress increases, the specimen tends to fail, and the crack expansion is rapid, ultimately reaching its peak strength.

3.2. Impact of Seepage Pressure on Deformation and Strength Parameters

In light of test results under the hydro-mechanical properties, we can see that the seepage pressure has a major affection on granite gneiss strength and deformation parameters under the hydro-mechanical properties. Basing the identical confining pressure, rising seepage pressure, rock peak strength, elastic modulus, and deformation modulus gradually appear to be a prominent decreasing trend. This is the confining pressure unloading effect. In accordance with the principle of effective stress, the larger the seepage pressure, the lower the actual confining pressure. Furthermore, the elastic modulus decrease rate takes on a declining trend with the seepage pressure rising, while the deformation modulus decrease rate appears an increasing inclination along with the seepage pressure increase. Observed this rock mechanical behavior characteristic evolution under compression in similar research [27,28].

In the same confining pressure, the yield strength changing its trend in pace with the seepage pressure increase is not obvious. This is because the development and closure of microcracks are very limited and can be ignored in linear elastic deformation as the rock specimen is mainly subjected to pressure from the rock skeleton, and the infiltration of permeable water would also be limited at this stage. The seepage water mainly couples seepage and stress through the flow of microcracks in the rock specimen. Compared with the confining pressure influence, the pore pressure affection on yield strength is very limited.

The experimental rock specimen was processed from the rock specimen drilled during exploration, which is often disturbed by large machinery and external forces in the early stage. The initial internal damage is unknown, and there is a certain possibility of dispersion. And the axial peak strain is closely bound up with the mechanical parameters, that is, the sample peak strength and elastic modulus. A weakening effect on the pore pressure to peak axial strain appears to have poor regularity, which is different from the trend of gradually decreasing parameters, that is, the peak strength as pore pressure rises. The yield axial strain appears to have a gradual growth trend with the pore pressure increasing.

3.3. Permeability Evolution Law of Granite Gneiss

In view of the granitic gneiss triaxial test results on the affection of hydro-mechanical properties, the granitic gneiss generally experiences three stages before the peak failure, namely the early stage of microcrack compaction, linear elastic deformation, and internal damage expansion and deformation failure. Volume strain is a parameter of the rock's overall deformation characteristics in triaxial tests that can be used to represent the rock samples' overall deformation characteristics under different stresses. The calculation formula for volumetric strain is shown in Equation (2).

$$\varepsilon_v = -\Delta V/V_0 = \varepsilon_1 + 2\varepsilon_3, \quad (2)$$

In the equation, ε_1 , ε_3 , ε_v , respectively are axial strain, circumferential strain, and volumetric strain, where ε_3 has negative values; ΔV is the increase in sample volume; and V_0 is the sample original volume. Figure 3 shows permeability and stress–volumetric strain curves in the coupling effect of hydro-mechanical properties.

The permeability evolution laws of rocks under different stress are different, and there is currently no unified model that can indicate the relevance between rocks' permeability and total stress–strain in diverse stress states. As seen in Figure 3, there is a good correlation between volume strain and permeability of granite gneiss in testing. Therefore, the granite gneiss hydro-mechanical properties model can be further established by discussing the relevance between its permeability and volume strain. The curve in the figure shows that the volumetric strain from point O to point A is the microcrack compaction initial stage. Permeability declines in the volumetric strain. Point A to point B is part of the linear elastic deformation stage, and the permeability appears to have a weak decreasing trend with the volume strain increasing or fluctuating around a fixed value; point B to point C is the

internal damage expansion and deformation failures stage, during which the permeability appears a major increasing trend with the volume strain changing.

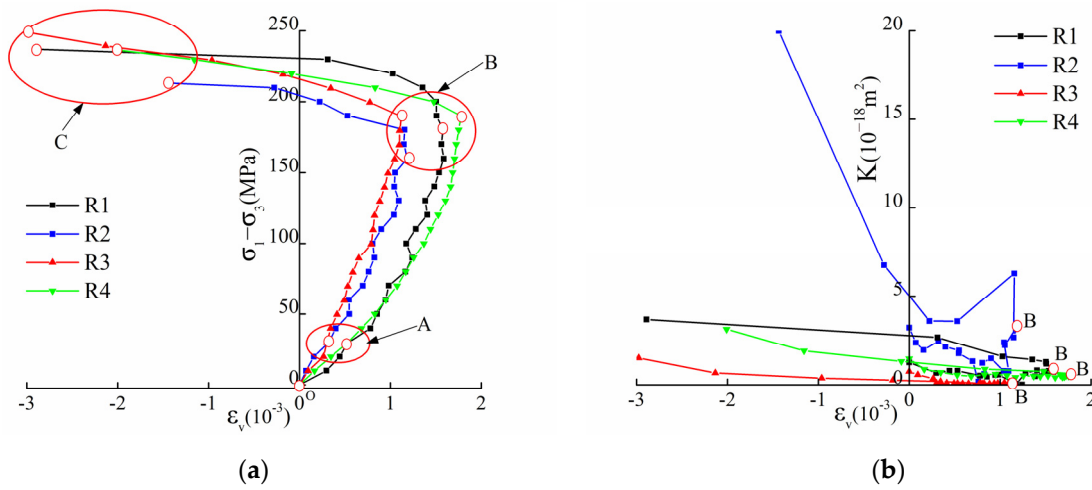


Figure 3. Permeability and stress–volumetric strain curves of granite gneiss: (a) stress–volumetric strain curves; (b) permeability–volumetric strain curves.

Point B is the boundary point that transitions from elastic deformation to plastic deformation, and it is also the peak point of volumetric strain, namely the volumetric expansion point. The permeability of rock samples R1 and R2 increase significantly after point B, while those of rock samples R3 and R4 do not increase as much, mainly because the confining pressure effectively enhances these rock samples ductility characteristics, as well as effectively restricts their lateral deformation and microcrack expansion. The higher the confining pressure, the lower the permeability of the rock samples. It is in accordance with the conclusions obtained in analogous research [29]. It is also the critical point for the expansion and enhancement of cracks in the rock and the transition of permeability from stable fluctuations to stable growth. Therefore, the granite gneiss permeability volume strain curve can be divided into two stages by taking point B as the dividing point. One stage is the gradual decrease in permeability, followed by a slight rate of decrease or fluctuations around a certain value. Another stage is when the rock specimen undergoes plastic deformation, and the permeability little by little increases with the volumetric strain changing, finally reaching its peak. In order to further analyze the permeability characteristics in the mechanical characteristics test in the coupling effect of hydro-mechanical properties, a function fitting method was used to study the two stages bounded by point B. Among them, the BC stage was analyzed using the volumetric strain relative value, as shown in Equation (3):

$$\varepsilon_{vi} = \varepsilon_{vB} - \varepsilon_v, \tag{3}$$

In the formula, ε_{vi} is the volumetric strain relative value in stage BC; ε_{vB} is the volumetric strain value at point B; ε_v is the actual volumetric strain value for stage BC.

Figure 4 shows the piecewise fitting relationship curve of permeability–volumetric strain in testing the hydro-mechanical properties. It can be seen that an exponential function can better fit the permeability change characteristics in section OB, while a logarithmic function is required for section BC to better simulate the permeability variation law with volume strain. A relevance between permeability and volumetric strain could be well demonstrated through piecewise fitting (sections OB and BC) so that the hydro-mechanical properties model can be established. The coupling expression is the following:

$$K = \begin{cases} y = a_1 \exp(-b_1 \varepsilon_v) + c_1 & (t < t_B) \\ y = a_2 \ln(\varepsilon_{vB} - \varepsilon_v + b_2) & (t \geq t_B) \end{cases}, \tag{4}$$

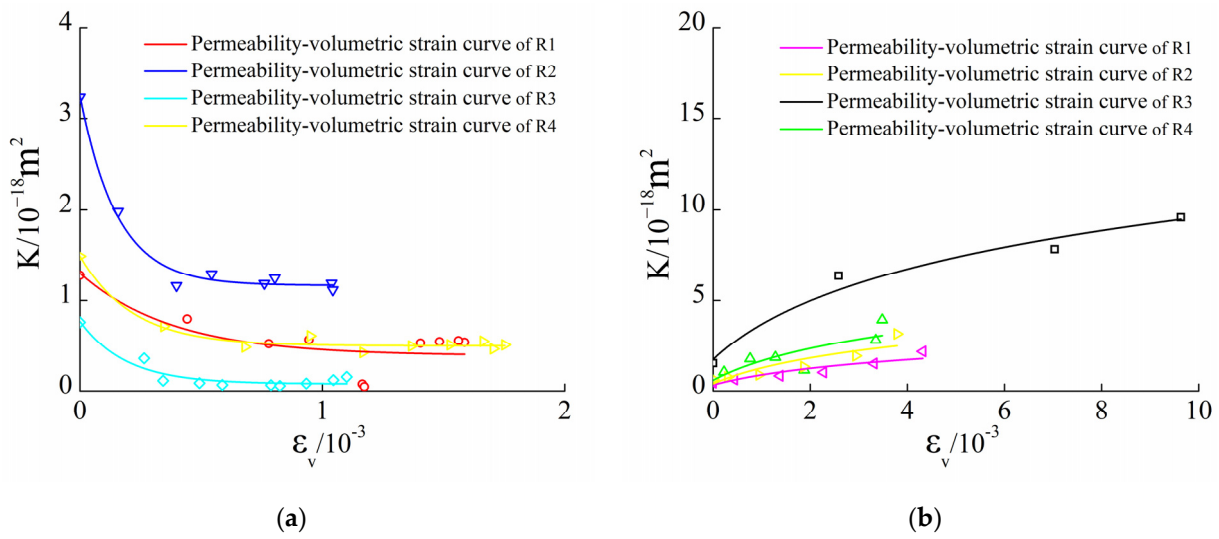


Figure 4. Triaxial compression tests permeability–volumetric strain curves: (a) section OB; (b) section BC.

In Formula (4), $a_1, b_1, c_1, a_2, b_2,$ and c_2 are experimental parameters, which can be fitted by the results of the hydro-mechanical properties test, as shown in Table 3.

Table 3. Permeability–volumetric strain curves fitting results.

Rock Specimen	Fitting Results				
	a_1	b_1	c_1	a_2	b_2
R1	0.912	2.592	0.389	2.142	1.645
R2	2.082	6.452	1.165	9.331	1.423
R3	0.692	5.268	0.077	0.618	0.870
R4	0.991	4.599	0.499	1.532	1.253

4. Numerical Simulation

4.1. Proposal of Coupling Variables

During the rock deformation and failure stage, there is relevance in the sample plastic deformation and the rock porosity changes. Entering the internal damage expansion, deformation, and failure stage, a relevance between the rock expansion caused volume porosity variations and the rock-generated plastic deformation. Rubin et al. established a correlation formula between plastic strain increment and expansion porosity increment [30,31]. An equation was proposed for the relation in the variation rate on expansion porosity and strain increment. This equation applies to porous media:

$$d\phi_{dil} = \frac{m_d q (\phi_{dil}^{max} - \phi_{dil}) d\epsilon_p}{p}, \tag{5}$$

In Equation (5), ϕ_{dil}^{max} is the expanding porosity maximum threshold, m_d is the rock expansion rate, q is the rock deviatoric stress, p is the average stress. Rock expansion porosity is 0 in the linear elastic stage. During the plastic deformation stage, the deviatoric stress and plastic deformation increments are positively correlated with the expansion porosity increment.

In accordance with the porous media theory, the instantaneous water infiltrating volume permeate ΔV_l (m^3) inner the rock is obtained as the Formula (6):

$$\Delta V_l = \frac{A_s \Delta p \Delta t}{\mu_l L_s} K, \tag{6}$$

In line with the relevance equation between volume strain and permeability in the granite gneiss hydro-mechanical properties test, the volume strain can be used to characterize permeate volume immersed into the rock specimen at any instant, so Formula (6) can be rewritten as Formula (7):

$$\Delta V_l = \begin{cases} \frac{A_s \Delta p \Delta t}{\mu_l L_s} (a_1 \exp(-b_1 \varepsilon_v) + c_1) & (t < t_B) \\ \frac{A_s \Delta p \Delta t}{\mu_l L_s} a_2 \ln(\varepsilon_v^{\max} - \varepsilon_v + b_2) & (t \geq t_B) \end{cases}, \quad (7)$$

where t_B is the dilatancy point of volume strain and the permeability expressed in exponential function and logarithmic function in the volume compression and dilatancy stage.

The permeable water affection is primarily reflected in water pressure on rock specimens' internal microcracks and pores. With regard to saturated rocks, the water influence on the rock stress field can be expressed by the ratio of permeability rate to pore water volume, defined as coupled variable ζ with the aim of demonstrating the impact on water instantaneous infiltration, as shown in Equation (8):

$$\zeta = \frac{\Delta V_l}{A_s L_s \phi'} \quad (8)$$

Formula (8) is the coupling variable expression we define. The rock volume strain, plastic strain, and deviatoric stress changes directly affect the coupled variable. In the meanwhile, the coupled variable under these influences will, in turn, transform the volume strain, plastic strain, and other variables, as well as achieve its coupling characteristic.

4.2. Establishment of Constitutive Model

Conventional linear failure surfaces cannot accurately indicate the nonlinear features of the rock sample. On account of the test analysis, an improved Durkcer–Prager criterion was used as the plastic yield function, and a hydro-mechanical properties variable was introduced into this equation to realize the characteristics of the sample hydro-mechanical properties [32–34]. This model simulates rocks as isotropic porous media. The improved equation is expressed as follows:

$$f = q^2 + A_0(1 - \alpha \zeta)h(\theta)\alpha_p(p - C_0)p_0 = 0, \quad (9)$$

In Formula (9), parameters A and C_0 in the plastic yield surface are obtained from different confining pressure conditions triaxial tests, ζ is the coupling variable, and α is the coefficient of the coupling variable.

The plastic potential energy can determine the incremental characteristics of plastic strain under the permeate action. In line with the relevant research results of S. Pietruszczak et al. [35]. The plastic potential energy equation in elastic–plastic damage constitutive model is improved by introducing the coupling variable:

$$g = q + A_0(1 - \alpha_1 \zeta)(1 - d)\eta h(\theta)(p - C_0) \ln\left(\frac{p - C_0}{I_0}\right) = 0, \quad (10)$$

In Formula (10), the intersection of the mean stress and plastic potential surface is I_0 , η is the volume compression and expansion points slope.

Damage occurs and expands continuously under the action of damage-driving forces. This study introduces a damage criterion proposed by J. Mazars [36] to characterize the granitic gneiss damage evolution.

$$f_d(Y_d^p, d) = d_c \tanh(B_d Y_d^p) - d \leq 0, \quad (11)$$

In Equation (11), Y_d^p is the rock damage driving force, d_c is the maximum damage variable, B_d controls the damage evolution rate.

The coupling effect on rocks could lead to degradations in the modulus of rock materials. Based on irreversible thermodynamic characteristics, the stiffness tensor can be obtained. The following expression of the stress–strain relationship is obtained:

$$\sigma = (1 - \alpha_2 \xi)(1 - d)\mathbb{C}^0 : \varepsilon^e = \mathbb{C}(\xi, d) : \varepsilon^e, \tag{12}$$

In Formula (12), it can be seen that both the coupled variables of seepage stress and damage can lead to the degradation of rock stiffness. In the test, degradations in the moduli are the result of the combined coupling effect, which is a non-increasing function. When coupling variables ξ and the damage variable d are both 0, the rock is in an initial state of no seepage and no damage, and the hydro-mechanical properties elastic stiffness matrix $\mathbb{C}(\xi, d)$ is the same as the initial elastic stiffness matrix \mathbb{C}^0 .

According to the consistency principle, considering that granite gneiss failure and nonlinear behavior is the result of damage, plastic deformation, and hydro-mechanical properties, listing the consistency conditions of damage, plasticity, and coupling. The damage multiplier dd can be obtained as shown in Equation (13):

$$\begin{aligned} dd &= -\frac{\partial f_d}{\partial Y_d^p} \left(\frac{\partial Y_d^p}{\partial \varepsilon^p} : d\varepsilon^p + \frac{\partial Y_d^p}{\partial \gamma_p} d\gamma_p \right) / \frac{\partial f_d}{\partial d} \\ &= -\lambda_s \frac{\partial f_d}{\partial Y_d^p} \left(\frac{\partial Y_d^p}{\partial \varepsilon^p} : \frac{\partial g}{\partial \sigma} + \frac{\partial Y_d^p}{\partial \gamma_p} \right) / \frac{\partial f_d}{\partial d} \end{aligned} \tag{13}$$

By substituting the damage multiplier dd into the coupling consistency condition, Equation (14) is obtained as follows:

$$d\xi = -\lambda_s \left(\frac{\partial \xi}{\partial d} : \frac{\partial f_d}{\partial Y_d^p} \left(\frac{\partial Y_d^p}{\partial \varepsilon^p} : \frac{\partial g}{\partial \sigma} + \frac{\partial Y_d^p}{\partial \gamma_p} \right) / \frac{\partial f_d}{\partial d} + \frac{\partial \xi}{\partial \varepsilon^p} : \frac{\partial g}{\partial \sigma} \right) + \frac{\partial \xi}{\partial \sigma} : d\sigma, \tag{14}$$

By substituting the coupled plastic flow law, damage multiplier, and hydro-mechanical properties multiplier into the plastic consistency condition, the coupled plastic multiplier λ_s can be obtained as Equation (15):

$$\lambda_s = \frac{\left(\frac{\partial f_s}{\partial \sigma} + \frac{\partial f_s}{\partial \xi} \frac{\partial \xi}{\partial \sigma} \right) d\sigma}{H_{\xi d}}, \tag{15}$$

Among the terms, $H_{\xi d}$ is the plastic hardening modulus, which is obtained as Equation (16):

$$\begin{aligned} H_{\xi d} &= \left(\frac{\partial f_s}{\partial d} + \frac{\partial f_s}{\partial \xi} \frac{\partial \xi}{\partial d} \right) \left(\frac{\partial f_d}{\partial Y_d^p} \left(\frac{\partial Y_d^p}{\partial \varepsilon^p} : \frac{\partial g}{\partial \sigma} + \frac{\partial Y_d^p}{\partial \gamma_p} \right) / \frac{\partial f_d}{\partial d} \right) \\ &\quad - \left(\frac{\partial f_s}{\partial \alpha_p} \frac{\partial \alpha_p}{\partial \gamma_p} + \frac{\partial \xi}{\partial \varepsilon^p} : \frac{\partial g}{\partial \sigma} \right) \end{aligned} \tag{16}$$

The hydro-mechanical properties multiplier $d\xi$, damage multiplier dd , and plastic multiplier λ_s are the key intermediate functions of the constitutive model. They respectively represent granite gneiss hydro-mechanical properties, the damage evolution rules, and the plastic deformation characteristics on the hydro-mechanical properties test.

4.3. Model Validation

Parameters A and C_0 in the plastic yield surface are obtained from different confining pressure conditions triaxial tests in order to obtain the trajectories of each rock specimen peak strength, where $A_0 = 950$ and $C_0 = 18$ MPa. The parameter $\eta = 0.021$ in the plastic hardening function is a parameter describing the initial yield surface position. The parameter $B = 0.0005$ of another plastic hardening function is obtained by plotting the function α_p and the plastic shear strain γ_p curve. $\eta = -0.0025$, which is the slope of the rock specimen compression and expansion area boundary line and is also the value corresponding to the plastic volume compression and expansion critical point. It could be specifically determined

by the volume expansion point of the granite gneiss triaxial mechanical property test. The critical values of damage variables, and for calculating and simulating the conveniently, $d_c = 0.9$ and $B_d = 125$ are taken. The coupling variable coefficients α , α_1 , and α_2 are all 1. The basic parameters in the coupling variables are all test parameters. Based on the research on the relationship between permeability and volume strain, the values are shown in Table 3.

In line with the establishment of the constitutive model and parameters determination, the mechanical characteristic test curve numerical simulation under the hydro-mechanical properties was carried out. The comparison between the simulation results and experimental data is shown in Figure 5.

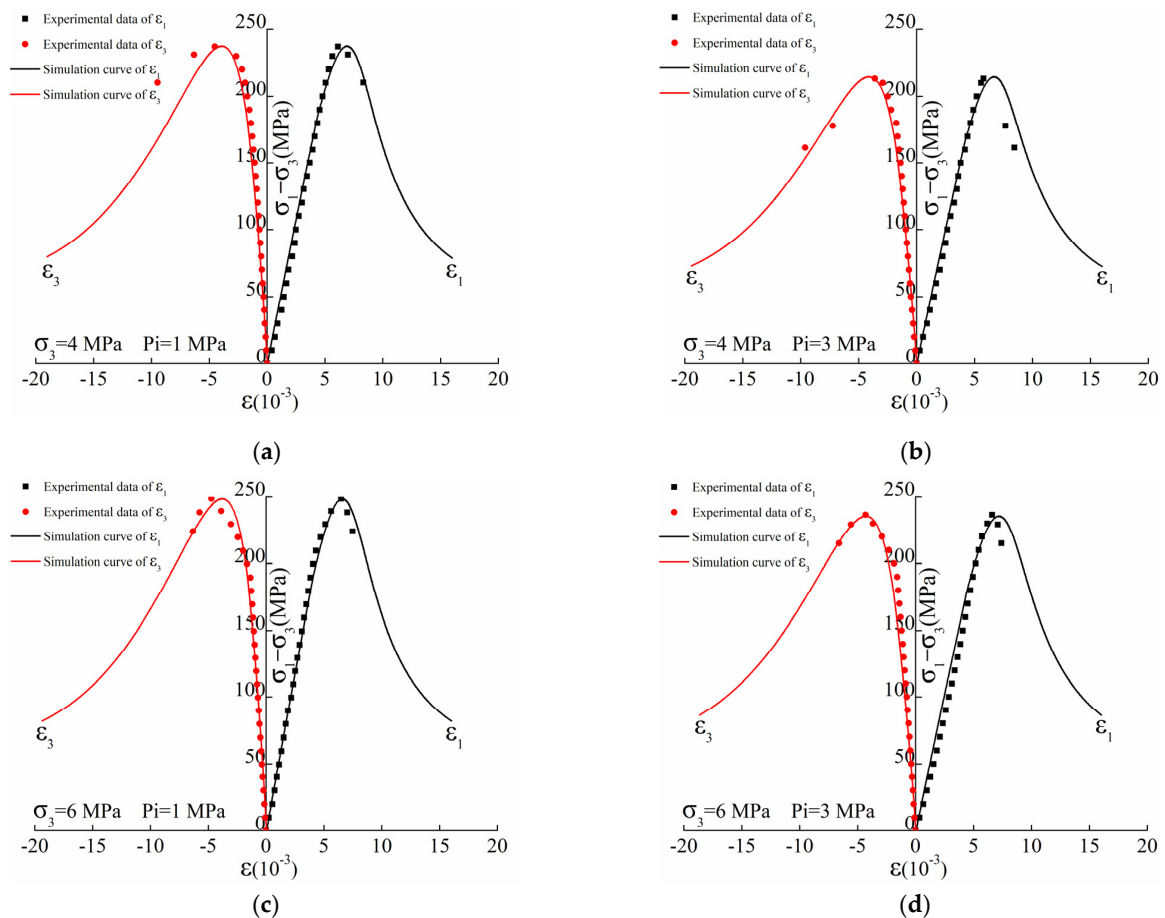


Figure 5. Simulation of triaxial compression tests of granite gneiss: (a) $\sigma_3 = 4$ MPa, $P_i = 1$ MPa; (b) $\sigma_3 = 4$ MPa, $P_i = 3$ MPa; (c) $\sigma_3 = 6$ MPa, $P_i = 1$ MPa; (d) $\sigma_3 = 6$ MPa, $P_i = 3$ MPa.

It is obtained from Figure 5 that the constitutive model would better simulate the granite gneiss triaxial test curve. Verification shows the results in the numerical and experimental match well. All peak strengths of rock samples R1 to R4 obtained by simulation are 237.56 MPa, 214.48 MPa, 248.91 MPa, and 235.82 MPa, respectively. Compared with the experimental data in Table 2, the differences are 0.18%, 0.59%, 0.06%, and 0.36%, respectively, none of which exceed 1%. And the simulated axial peak strains of rock samples R1 to R4 are 6.38, 6.05, 6.55, and 6.93, respectively. Compared with the experimental data in Table 2, the differences are 4.08%, 4.85%, 0.92%, and 4.84%, respectively, all of which do not exceed 5%. The established hydro-mechanical properties constitutive model can not only describe the plastic deformation, damage evolution, pressure dependence, compression to dilatancy transition, pre-peak plastic hardening, and post-peak strain softening of granite gneiss but also describe the changes in deformation and strength characteristics under different seepage pressure conditions. This model would better interpret the granite gneiss hydro-mechanical properties under seepage water pressure.

5. Conclusions

In this research, the granite gneiss mechanical properties under hydro-mechanical properties were studied experimentally. A fully automatic triaxial servo system for rock was used to conduct triaxial mechanical tests under hydro-mechanical properties. There are several conclusions as follows:

- (1) The results divide the stress–strain process into three stages to characterize rock materials' mechanical behavior characteristics under triaxial compression conditions. (i) The microcrack compaction stage is a relatively small nonlinear deformation stage on the rock's internal microcracks and pores under stress. (ii) The linear elastic deformation stage is mainly affected by the pressure of the rock skeleton. Its linear slope is the rock elastic modulus, which is a vital parameter for characterizing mechanical properties. (iii) The damage and failure stage is a nonlinear plastic deformation stage where cracks expand rapidly.
- (2) The boundary point between the first and second stages generally distributes around the first intersection of the stress–strain curve and the permeability–strain curve. The volumetric expansion point is the peak value of volumetric strain, which is the dividing point in the second and third stages, identified from the volume stress–strain curve. The granite gneiss hydro-mechanical properties model can be established by the piecewise fitting curve.
- (3) In view of the experimental data, a hydro-mechanical properties constitutive model that is suitable for isotropic porous media was built to model the granite gneiss mechanical behavior under different seepage pressure conditions. To test the model's reliability, compare the numerical and experimental results. The simulated peak strengths of rock samples R1 to R4 were determined to be 237.56 MPa, 214.48 MPa, 248.91 MPa, and 235.82 MPa, respectively. Compared with the experimental data, all of these were less than 1%. The axial peak strains were 6.38, 6.05, 6.55, and 6.93, respectively. Compared with the experimental data, all of these were less than 5%. The two datasets match well, which proves this model can offer a good representation of the rock behavior prominent distinctions, that is, the plastic deformation, material damage, and hydro-mechanical properties, in different seepage pressure conditions.

The constitutive model could describe the mechanical behavior characteristics of deep-buried hard rock under the coupling effect and has important engineering value in describing rock mechanics and for underground structural safety research. In future studies, further tests on various rocks should be conducted with more loading conditions for the purpose of verifying the preliminary conclusions drawn in this research. Important value could be provided for the major national infrastructure projects' long-term stability and safety, for instance, large-scale water conservancy and hydropower projects, as well as underground energy storage and transportation projects in complex environments.

Author Contributions: Conceptualization, L.L.; methodology, L.L.; software, B.W.; validation, L.L. and B.W.; formal analysis, L.L.; investigation, L.L. and B.W.; resources, L.L.; data curation, L.L.; writing—original draft preparation, L.L.; writing—review and editing, B.W.; visualization, L.L.; supervision, B.W.; project administration, L.L. and B.W.; funding acquisition, L.L. and B.W. All authors have read and agreed to the published version of the manuscript.

Funding: This research was funded by the Natural Science Foundation of Jiangsu Province, grant number BK20191302, and the Natural Science Foundation of Jiangsu Higher Education Institutions of China, grant number 22KJB560026.

Institutional Review Board Statement: Not applicable.

Informed Consent Statement: Not applicable.

Data Availability Statement: Data are contained within the article.

Conflicts of Interest: The authors declare no conflict of interest.

References

1. Yang, S.Q.; Huang, Y.H.; Jiao, Y.Y.; Zeng, W.; Yu, Q.L. An experimental study on seepage behavior of sandstone material with different gas pressures. *Acta Mech. Sinica* **2015**, *31*, 837–844. [[CrossRef](#)]
2. Jing, L.R.; Feng, X.T. Numerical modeling for coupled thermo-hydro-mechanical and chemical processes (THMC) of geological media-international and Chinese experiences. *Chin. J. Rock Mech. Eng.* **2003**, *22*, 1704–1715.
3. Yin, Q.; Wu, J.Y.; Jiang, Z.; Zhu, C.; Su, H.; Jing, H.; Gu, X. Investigating the effect of water quenching cycles on mechanical behaviors for granites after conventional triaxial compression. *Geomech. Geophys. Geo-Energy Geo-Resour.* **2022**, *8*, 77. [[CrossRef](#)]
4. Figueiredo, B.; Tsang, C.F.; Rutqvist, J.; Niemi, A. A study of changes in deep fractured rock permeability due to coupled hydro-mechanical effects. *Int. J. Rock Mech. Min. Sci.* **2015**, *79*, 70–85. [[CrossRef](#)]
5. Chen, J.; Zhao, J.; Zhang, S.; Zhang, Y.; Yang, F.; Li, M. An experimental and analytical research on the evolution of mining cracks in deep floor rock mass. *Pure Appl. Geophys.* **2020**, *177*, 5325. [[CrossRef](#)]
6. Lin, L.; Xu, W. Experimental Researches on Long-Term Strength of Granite Gneiss. *Adv. Mater. Sci. Eng.* **2015**, *2015*, 187616.
7. Yasuhara, H.; Kinoshita, N.; Ogata, S.; Cheon, D.S.; Kishida, K. Coupled thermo-hydro-mechanical-chemical modeling by incorporating pressure solution for estimating the evolution of rock permeability. *Int. J. Rock Mech. Min. Sci.* **2016**, *86*, 104–114. [[CrossRef](#)]
8. Yang, S.Q.; Jing, H.W. Evaluation on strength and deformation behavior of red sandstone under simple and complex loading paths. *Eng. Geol.* **2013**, *164*, 1–17. [[CrossRef](#)]
9. Yang, S.Q.; Jing, H.W.; Cheng, L. Influences of pore pressure on short-term and creep mechanical behavior of red sandstone. *Eng. Geol.* **2014**, *179*, 10–23. [[CrossRef](#)]
10. Liu, L.; Xu, W.Y.; Wang, H.L.; Wang, W.; Wang, R.B. Experimental studies on hydro-mechanical properties of metamorphic rock under hydraulic pressures. *Eur. J. Environ. Civ. Eng.* **2016**, *20*, 45–59. [[CrossRef](#)]
11. Chen, H.Z.; Shao, Z.S.; Jin, D.D.; Zhang, Z.; Zhou, D.B. A numerical investigation into the effect of homogeneity on the time-dependent behavior of brittle rock. *Materials* **2021**, *14*, 6818. [[CrossRef](#)] [[PubMed](#)]
12. Uchida, S.; Klar, A.; Yamamoto, K. Sand production model in gas hydrate-bearing sediments. *Int. J. Rock Mech. Min. Sci.* **2016**, *86*, 303–316. [[CrossRef](#)]
13. Menaceur, H.; Delage, P.; Tang, A.M.; Conil, N. The thermo-mechanical behaviour of the Callovo-Oxfordian claystone. *Int. J. Rock Mech. Min. Sci.* **2015**, *78*, 290–303. [[CrossRef](#)]
14. Wang, Z.; Li, S.; Qiao, L.; Zhang, Q. Finite element analysis of the hydro-mechanical behavior of an underground crude oil storage facility in granite subject to cyclic loading during operation. *Int. J. Rock Mech. Min. Sci.* **2015**, *73*, 70–81. [[CrossRef](#)]
15. Zhang, Z.L.; Xu, W.Y.; Wang, W.; Wang, R.B. Triaxial creep tests of rock from the compressive zone of dam foundation in Xiangjiaba Hydropower Station. *Int. J. Rock Mech. Min. Sci.* **2012**, *50*, 133–139. [[CrossRef](#)]
16. Zhao, J.; Feng, X.T.; Yang, C.; Zhou, Y.; Zhang, Y. Study on time-dependent fracturing behaviour for three different hard rock under high true triaxial stress. *Rock Mech. Rock Eng.* **2021**, *54*, 1239–1255. [[CrossRef](#)]
17. Zuo, J.P.; Wei, X.; Wang, J.; Liu, D.J.; Cui, F. Investigation of failure mechanism and model for rocks in deep roadway under stress gradient effect. *J. China Univ. Min. Technol.* **2018**, *47*, 478–485.
18. Liu, L.; Xu, W.Y.; Wang, H.L.; Wang, W.; Wang, R.B. Permeability evolution of granite gneiss during triaxial creep tests. *Rock Mech. Rock Eng.* **2016**, *49*, 3455–3462. [[CrossRef](#)]
19. Zhang, Y.; Shao, J.F.; Xu, W.Y.; Zhao, H.B.; Wang, W. Experimental and numerical investigations on strength and deformation behavior of cataclastic sandstone. *Rock Mech. Rock Eng.* **2015**, *48*, 1083–1096. [[CrossRef](#)]
20. Chen, L.; Wang, C.P.; Liu, J.F.; Liu, J.; Wang, J.; Jia, Y.; Shao, J.F. Damage and plastic deformation modeling of beishan granite under compressive stress conditions. *Rock Mech. Rock Eng.* **2015**, *48*, 1623–1633. [[CrossRef](#)]
21. Wang, X.; Song, L.; Xia, C.; Han, G.; Zhu, Z. Nonlinear elasto-visco-plastic creep behavior and new creep damage model of dolomitic limestone subjected to cyclic incremental loading and unloading. *Sustainability* **2023**, *13*, 12376. [[CrossRef](#)]
22. Yang, S.Q.; Jiang, Y.Z. Triaxial mechanical creep behavior of sandstone. *Min. Sci. Technol.* **2010**, *20*, 339–349. [[CrossRef](#)]
23. Hu, B.; Yang, S.; Xu, P. A nonlinear rheological damage model of hard rock. *J. Cent. South Univ.* **2018**, *25*, 1665–1677. [[CrossRef](#)]
24. Ulusay, R.; Hudson, J.A. *The Complete ISRM Suggested Methods for Rock Characterization, Testing and Monitoring*; Springer: Ankara, Turkey, 2007.
25. Simmons, C.T. Henry Darcy (1803–1858): Immortalised by his scientific legacy. *Hydrogeol. J.* **2008**, *16*, 1023–1038. [[CrossRef](#)]
26. Wang, J.A.; Park, H.D. Fluid permeability of sedimentary rocks in a complete stress–strain process. *Eng. Geol.* **2002**, *63*, 291–300. [[CrossRef](#)]
27. Zhang, Y.; Liu, Z.B.; Xu, W.Y.; Shao, J.F. Change in the permeability of clastic rock during multi-loading triaxial compressive creep tests. *Geotech. Lett.* **2015**, *5*, 167–172. [[CrossRef](#)]
28. Heiland, J. Laboratory testing of coupled hydro-mechanical processes during rock deformation. *Hydrogeol. J.* **2013**, *11*, 122–141. [[CrossRef](#)]
29. Palchik, V. Is there link between the type of the volumetric strain curve and elastic constants, porosity, stress and strain characteristics? *Rock Mech. Rock Eng.* **2013**, *46*, 315–326. [[CrossRef](#)]
30. Morris, J.P.; Lomov, I.N.; Glenn, L.A. A constitutive model for stress-induced permeability and porosity evolution of Berea sandstone. *J. Geophys. Res. Solid Earth* **2003**, *108*, 237. [[CrossRef](#)]

31. Rubin, M.B.; Vorobiev, O.Y.; Glenn, L.A. Mechanical and numerical modeling of a porous elastic–viscoplastic material with tensile failure. *Int. J. Solids Struct.* **2000**, *37*, 1841–1871. [[CrossRef](#)]
32. Liu, L.; Xu, W.Y.; Zhao, L.Y.; Zhu, Q.Z.; Wang, R.B. An experimental and numerical investigation of the mechanical behavior of granite gneiss under compression. *Rock Mech. Rock Eng.* **2017**, *50*, 499–506. [[CrossRef](#)]
33. Shao, J.F.; Zhu, Q.Z.; Su, K. Modeling of creep in rock materials in terms of material degradation. *Comput. Geotech.* **2003**, *30*, 549–555. [[CrossRef](#)]
34. Shao, J.F.; Chau, K.T.; Feng, X.T. Modeling of anisotropic damage and creep deformation in brittle rocks. *Int. J. Rock Mech. Min. Sci.* **2006**, *43*, 582–592. [[CrossRef](#)]
35. Pietruszczak, S.; Jiang, J.; Mirza, F.A. An elastoplastic constitutive model for concrete. *Int. J. Solids Struct.* **1988**, *24*, 705–722. [[CrossRef](#)]
36. Mazars, J. A description of micro-and macroscale damage of concrete structures. *Eng. Fract. Mech.* **1986**, *25*, 729–737. [[CrossRef](#)]

Disclaimer/Publisher’s Note: The statements, opinions and data contained in all publications are solely those of the individual author(s) and contributor(s) and not of MDPI and/or the editor(s). MDPI and/or the editor(s) disclaim responsibility for any injury to people or property resulting from any ideas, methods, instructions or products referred to in the content.